AN ABSTRACT OF THE THESIS OF

David M. McCreary for the degree of Master of Science in Nuclear Engineering presented on October 26, 2000. Title: Design and Testing of Intrusive Conductivity Probes For the Measurement of Two-Phase Flow Parameters.

Redacted for Privacy

Abstract approved:______________________________________

Qiao Wu.

This thesis examines two techniques for measuring two-phase flow parameters in an air/water system using intrusive conductivity probes. Specifically, the theoretical derivation for measuring void fraction and interfacial area using a two-sensor needle-type probe is derived, and a statistical analysis of the accuracy using the two-sensor probe for measuring interfacial area will be determined from a comprehensive literature review. The second technique used to measure void fraction in air/water flows is with a half-ring type conductivity probe. This half-ring type probe measures an area-averaged void fraction, while the needle-type probe measures local two-phase parameters. A single-sensor needle-type probe is used to experimentally measure void fraction in a test section, and is then benchmarked with another instrument as well as the drift-flux model. The half-ring type probe is then cross-calibrated with the needle-type probe.

A complete system for measurement of local void fraction in an air/water two-phase mixture using two measurement techniques is presented. A detailed design procedure for a single-sensor conductivity probe as well as a half-ring type probe, and the corresponding circuits to power them are discussed. The two techniques discussed are accurate, simple, reliable, and inexpensive.

Design and Testing of Intrusive Conductivity Probes

For the Measurement of Two-Phase Flow Parameters

by

David M. McCreary

A THESIS

submitted to

Oregon State University

in partial fulfillment of
the requirements for the
degree of

Master of Science

Completed October 26, 2000
Commencement June 2001

Master of Science of David M. McCreary presented on October 26, 2000

APPROVED:

Redacted for Privacy

Major Professor, representing Nuclear Engineering

Redacted for Privacy

Chair of Department of Nuclear Engineering

Redacted for Privacy

Dean of Graduate School

I understand that my thesis will become part of the permanent collection of Oregon State University libraries. My signature below authorizes release of my thesis to any reader upon request.

Redacted for Privacy

David M. McCreary, Author

ACKNOWLEDGMENTS

Many people have given me help over the years; to all of them I say thank you. In particular, I wish to thank my advisor, Dr. Qiao Wu. It is a rare privilege to have a mentor who is so genuinely concerned with the well-being of his students while simultaneously being dedicated to his own research and field of study. He has opened every door of opportunity to me, giving me free reign to explore and learn but gently reigning me in at the right moments and providing all of the necessary answers when I was stuck. For his kindness and careful instruction, I am truly grateful. His brilliance will always be a source of inspiration for me.

I especially thank Dr. José Reyes, Jr., Principal Investigator of the Advanced Thermal Hydraulic Research Laboratory (ATHRL) for allowing me cutting-edge experimental research opportunities. ATHRL truly is a world-class thermal-hydraulic research facility that continues to set the standard in pioneering research work, quality assurance, and safety.

It would not be possible to have such a quality facility without many exceptional people. In particular, John Groome, Chris Gunderson, and Teresa Culver have insured the successful operation of ATHRL, in addition to offering me their professional and insightful help on many, many occasions. Thank you.

My parents could not have been more supportive. Their love and enthusiasm have made my education truly special. They have taught me from the very beginning and have been the most important source of motivation and encouragement. My family has provided the most loving environment possible and I am truly blessed to have grown up in such wonderful surroundings.

TABLE OF CONTENTS

TABLE OF CONTENTS (Continued)

Page

LIST OF FIGURES

LIST OF FIGURES (Continued)

NOMENCLATURE

Q volumetric flow rate
j superficial phase velocity
D mainline diameter
d branch diameter
ρ density
Fr Froude Number
V phase velocity
w mass flow rate
g acceleration due to gravity
h height

Subscripts

g gas phase
f, l liquid phase
b beginning of liquid entrainment
HL hot-leg
1 mainline
2 run
3 branch
$D_H^{\bullet}$ dimensionless hydraulic diameter of vessel
D diameter of vessel
V_{gj}^{+} dimensionless drift velocity
ρ mass density
Fr Froude Number
α void fraction
j_g gas flux
C_o distribution parameter
V_{gj} drift velocity

Operators

< > area-averaged
<< >> void-weighted, area-averaged

Design and Testing of Intrusive Conductivity Probes
For the Measurement of Two-Phase Flow Parameters

1. INTRODUCTION

This thesis focuses on the development and analysis of conductivity probes for the measurement of gas void fraction, bubble velocity, and interfacial area in two-phase air/water flows. Two styles of needle-type conductivity probes were designed and fabricated for the local measurement of these two-phase parameters. In addition, a half-ring-type conductivity probe was also designed and fabricated for applications in vertical and horizontal flows. Chapter 1 presents a brief introduction and addresses the significance and technical background of these probes, which leads to the identification of the thesis objectives.

1.1. Importance of Accurate Measurements for Two-Phase Flow Parameters

Two-phase flow through pipes and associated equipment is of particular interest in the petroleum and chemical processing industries, heat transfer equipment, and nuclear power plants. Two-phase flow is classically characterized by interfacial structures, called flow regimes. These flow regimes, in turn, have unique transport phenomena (e.g. pressure loss and heat transfer). Vertical two-phase flow regimes in pipes are typically divided into four basic flow regimes characterized as follows [1]:

(1) Bubbly Flow: Small, discrete bubbles (or distorted bubbles) that are surrounded by a continuous liquid medium.

(2) Slug Flow: Slugs of liquid and bubbles are separated by regions of high vapor content.

(3) Churn Flow: A highly chaotic flow regime in which the vertical motion of the two phases is oscillatory. The liquid phase is present in irregularly shaped fragments due to strong turbulent effects.

(4) Annular Flow: Gas vapor is flowing in the center of the pipe and the liquid partially as a film along the walls as well as droplets in the vapor region.

Flow regimes are typically identified from a flow regime map that is based on pipe geometry and liquid and gas volumetric fluxes. Constitutive relations have then been developed for each flow regime. The flow regime map is subjective however, and not suitable for transient conditions or flow inlet regions [2].

A more modern alternative to the traditional flow regime map is the three-dimensional two-fluid model. Each of the two phases has conservation equations governing the balance of mass, momentum and energy. Ishii and Mishima simplified the two-fluid model as follows [2]:

Continuity Equation:

$$\frac{\partial \alpha_k \rho_k}{\partial t} + \nabla \cdot (\alpha_k \rho_k \vec{v}_k) = \Gamma_k \tag{1.1}$$

Momentum Equation:

$$\frac{\partial \alpha_k \rho_k \vec{v}_k}{\partial t} + \nabla \cdot (\alpha_k \rho_k \vec{v}_k \vec{v}_k) = -\alpha_k \nabla p_k + \nabla \cdot \alpha_k \left(\bar{\tau}_k + \tau_k^t\right) + \alpha_k p_k \vec{g} + \vec{v}_{ki} \Gamma_k$$

$$+ \vec{M}_{ik} - \nabla \alpha_k \cdot \tau_i + (p_{ki} - p_k) \nabla \alpha_k \tag{1.2}$$

Enthalpy Energy Equation

$$\frac{\partial \alpha_k \rho_k H_k}{\partial t} + \nabla \cdot (\alpha_k \rho_k H_k \vec{v}_k) = -\nabla \cdot \alpha_k \left(\overline{q}_k + q_k^t\right) + \alpha_k \frac{D_k}{Dt} p_k$$

$$+ H_{ki}\Gamma_k + \frac{q_{ki}''}{L_s} + \phi_k \tag{1.3}$$

Where Γ_k, $\bar{M}_k$, τ_i, q_{ki}'', and ϕ_k are the mass generation rate density, generalized interfacial force per unit volume, interfacial shear stress, interfacial heat flux and dissipation rate, respectively. The subscript k denotes the k-phase, and i denotes the value at the interface. L_s is the length scale at the interface, and the inverse of this quantity is the interfacial area per unit volume (interfacial area concentration with a dimension of inverse length) [2]. The two-fluid model is applicable for transient analysis of two-phase systems. While the void fraction, α_k, is treated as a field variable, the interfacial area concentration, a_i, would ideally be known from another constitutive relation in the form of either a correlation or a transport equation. Correlations usually depend on flow regimes, resulting in artificial discontinuities and numerical instabilities [3, 4]. Therefore, Kocamustafaogullari and Ishii [5] generalized the population balance approach suggested by Reyes in order to obtain a closure transport equation (the interfacial area transport equation) for the two-fluid model. The two-fluid model treats flow regime transitions as the results of bubble coalescence and disintegration, and properly captures the dynamic nature of the evolving interfacial structure. Currently, a one-group model for the interfacial area transport equation pertaining to dispersed bubbles was recently devised by Wu et al [6].

However, a solid experimental database is needed to evaluate the two-fluid model along with its constitutive relations [7]. The most important parameters to be acquired for this purpose are void fraction, interfacial area concentration and the phase interface velocity, because there are no such comparable counterparts in single-phase flows. The measurement of local void fraction can be achieved with a needle-type single-sensor conductivity probe, which is not commercially available and thus constitutes one of the thesis tasks. The measurement of interfacial area concentration presents a great challenge to experimentalists due to its complicated relation with measurable variables. Ishii's work suggested that the time-averaged local interfacial area concentration is related to the harmonic mean of the bubble interface velocity in the outward normal direction of the bubble interface [8]. Since a needle-type double-sensor conductivity probe can measure both the local void fraction and interface velocity in a two-phase system, data from this type of probe can be used to validate not only the two-fluid model, but also the closure relation of interfacial area concentration [9]. Therefore, developing a double-sensor probe is another task of this thesis. In addition, a novel half-ring type conductivity probe has been designed and constructed for the measurement of area-averaged void fraction in vertical and horizontal two-phase flows, comprising the third contribution of this thesis.

1.2. Common Measurement Techniques

Accurate measurement of the local void fraction and interfacial area in a two-phase flow system is crucial to many industrial processes, and especially critical in nuclear reactor cooling systems. The data acquisition system and two conductivity probe designs outlined in this thesis will be used to measure the void fraction in the Oregon State University (OSU) Advanced Test Loop for Air-water Thermal-hydraulic Studies (ATLATS) facility. There are many options for local measurement of the void fraction such as the gamma densitometer, visualization, Magnetic Resonance Imaging (MRI), acoustic bubble spectroscopy, and the Laser Doppler Anemometer (LDA) [10, 11]. However, with the exception of the visualization technique, the systems are very expensive. Visualization and the LDA are limited to measuring low void fractions of approximately 20% and lower, and require a transparent test section. As the void fraction increases, sound and light waves require more energy to traverse the large number of air/water interfaces to reach the desired measurement volume with acoustic bubble. All of the above instruments are non-intrusive with the exception of the conductivity probes. The conductivity probes outlined in this thesis protrude into the flow field and cause flow disturbances. Despite this major drawback and the problems inherent with it, the single and double sensor probes as well as the half-ring probe remain the least expensive to operate, yet are still reliable and provide accurate data.

While the half-ring type probe is a relatively new concept, the needle-type probe has been in use for over thirty years though there is no commercially available product. There are a few derivatives of the needle-type probe, namely the single-sensor, double-sensor, and four-sensor probes. The latter two probes are used to calculate the local interfacial area by measuring the local bubble velocity. The single-sensor probe can only determine the local void fraction, while the double-sensor probe can measure a spherical bubble's velocity and relate this to the interfacial area concentration. The four-sensor probe is used in cap/slug bubble flow regimes to measure the bubble interface velocities and similarly compute the interfacial area. Only the single-sensor and double-sensor needle-type probe measurement techniques will be examined in the next few chapters.

For a detailed review on four-sensor probe measurement techniques, reference [12] is recommended.

1.3. Research Objectives

The objectives of this thesis are:

1. Design, construct, and process experimental data from a single-sensor conductivity probe to measure local void fraction in an air/water two-phase vertical test section.
2. Design and analyze the effectiveness of the two-sensor probe in measuring spherical bubble velocity, and therefore, interfacial area concentration in an air/water two-phase system.
3. Design, construct, and calibrate a half-ring conductivity probe to measure global void fraction in an air/water two-phase flow pipe system.

Chapter 2 of this thesis describes the fabrication procedure and data acquisition techniques to measure void fraction for the single-sensor probe, while Chapter 3 presents the results of an experimental effort to compare the measured void fraction from the single-sensor probe to other measurement tools and correlations. In Chapter 4, a discussion on the accuracy of measuring bubble velocity and interfacial area using a two-sensor probe is presented, while Chapter 5 gives an introduction to a half-ring probe. After cross-calibration with the single-sensor probe, the half-ring probe can measure area-averaged void fraction. Chapter 6 presents the drawbacks inherent with the two conductivity probe designs in this thesis and offers recommendations for future research. Chapter 7 sums up the thesis with conclusions from this research.

2. FABRICATION PROCEDURES AND DATA ACQUISITION TECHNIQUES FOR THE SINGLE-SENSOR CONDUCTIVITY PROBE

2.1. Measurement Theory of Needle-Type Probes

The intrusive electrical resistivity probe technique was first proposed by Neal and Bankoff in 1963 [13]. The single-sensor probe is shown below in Figure 1. For air-water systems, because the conductivity of air is less than the conductivity of water, the conductivity probe is designed so that the tip of the probe is at a different potential than the probe case (and therefore the conductive two-phase mixture). When a tip of the probe penetrates a bubble, a rise in the impedance is detected for the duration of time that the bubble takes to pass through that sensor tip. By obtaining the impedance signal from this tip, the local time-averaged void fraction can be obtained as:

$$\overline{\alpha}^{t} \equiv \frac{\sum \Delta t_{ki}}{T} \tag{2.1}$$

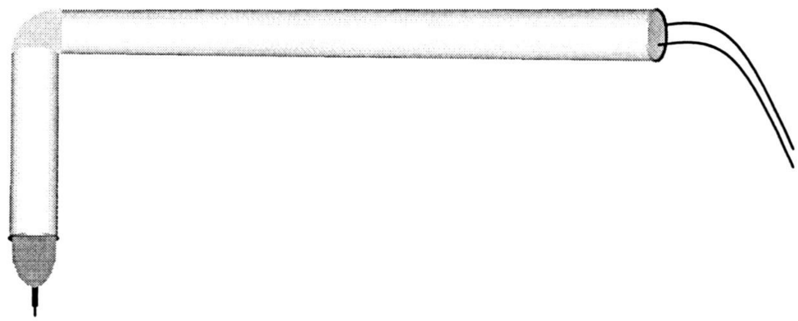

Figure 1. Double-sensor conductivity probe.

T is the total time measured, and Δt_{ki} is the time occupied by the gas phase.

This chapter describes a fabrication procedure for the OSU single-sensor conductivity probe, as well as the data acquisition tools used. The fabrication procedure outlined below is for a single-sensor probe. A double-sensor probe is fabricated in the same manner, except for the addition of another accupunctual needle and wire. The spacing between the two needles should follow the guidelines set in Chapter 4.

2.2. Fabrication Procedure

The single-sensor conductivity probe design outlined below is the culmination of many years of experimental effort by various researchers [9, 12-15]. This section describes the materials and fabrication procedure of a single-sensor conductivity probe – details of the necessary power circuit and data acquisition system are described later. The four key design parameters are performance; longevity; cost; and manufacturing time. The probe presented below is a derivative of Purdue University's successful double-sensor conductivity probe with a few new modifications [14]. The probe is designed to be as small and unobtrusive as possible, yet still be large and strong enough for multiple applications. Overall probe size will be dependent on the application. For measurements in the OSU ATHRL facility, the probe has an outer casing made of Ga 11 standard-wall stainless steel tubing. This Ga 11 OD is approximately 1/8th in. in diameter, so it may be used with common Swagelok™ teflon-ferreled fittings for easy movement in a test section. Many hours of testing has proved the probes' durability to water superficial velocities exceeding 3m/sec., yet the design presents a very small cross-sectional area to the flow. The tip itself is made of a stainless steel accupunctual needle (Ga. 00) from OMS Medical Supplies. The needle is crimped to a very thin copper wire (teflon-coated thermocouple wire), and then inserted into the stainless steel tubing. The needle and the outer casing form the two electrodes to complete the circuit. A procedure for making the probe shown in Figure 1 is outlined below. Note: If a particular application is at a very high flow rate, approximately 3m/sec or higher, the presented probe will experience a deflection and/or vibration. In these cases, the probe outer casing should be changed to a larger diameter, or thick-wall tubing used. Design constraints are listed in Chapter 4.

2.2.1. Materials and Tools

Most of the materials used were ordered from McMaster-Carr with the exception of the accupunctual needles and the teflon-coated thermocouple wire. The following materials and indicated quantity are suitable for constructing one single-sensor probe:

- Standard-Wall, Stainless Steel Micro Tubing: Part number 8987k41 has different Gauge options, sold in 1 ft. lengths at a price of ~$4 each. Ga. 11 and Ga. 14 tubes are needed, along with Ga. 27 tube.
- Stainless Steel Repair Kit: Part number 65985A11 is at a price of ~$10 per package.
- Copper Bond™ Epoxy
- Accupuncual Needles: SEIRIN needles are form OMS Medical Supplies (Ga. 02, 0.12 mm. diameter, 30 mm. long). J-type with tube package costs ~$12 (100 needles per package).
- Teflon-Coated Copper Thermocouple Wire: 0.005 inch O.D copper wire Part Number is TFCP-005-50 of OMEGA ENGINEERING, sold in 50foot spool (~$15)
- Buehler 4/0 Polishing Paper

- Dremel™ Grinder w/ Assortment of sanding bits
- Tweezers
- Razor Blade

2.2.2. Material Preparation

To construct one single-sensor probe, a few materials need to be prepared first. The stainless steel micro tubes (Ga. 11 and 14), and also the accupunctual needle need to be polished first with the Buehler polishing paper.

(a) Cut the Ga. 14 tube to a length of ~ 3inches with the Dremel.

(b) Using the thin cutting wheel on the Dremel, cut a slit in the Ga. 14 tube a little past the radius of the tube approximately 0.5 in. from one end as shown in Figure 2:

Figure 2. Preparation of Ga 14 tube.

(c) Next, cut a similar slit in the Ga. 11 tube approximately 1 in. from an end.

(d) Cut one piece of the thermocouple wire to a length of 1.5 ft.

(e) Using tweezers, strip ¼ in. of the teflon coating from both sides of the thermocouple wire. Ensure that the exposed copper wire does not become contaminated (which would increase the resistance).

(f) Cut the accupunctual needle handle off.

(g) Using a razor blade, gently roll the Ga. 27 tubing under the blade to cut a piece 0.5 in. long. Be careful not to deform the tubing since the thermocouple wire and needle needs to be inserted in it.

2.2.3. Assembly

(a) Insert the Ga. 14 tube into the Ga. 11 tube as shown in Figure 3, and align the slits together.

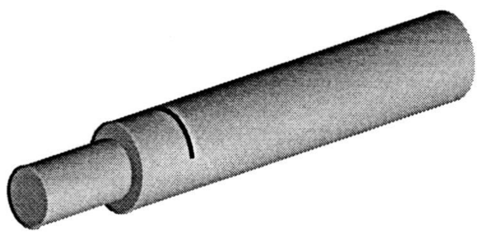

Figure 3. Alignment of Ga. 11 and 14 tubes.

(b) Bend the above group ninety degrees together as shown in Figure 4:

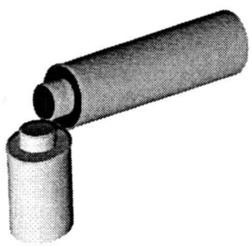

Figure 4. Ninety degree bend.

(c) Insert one end of the exposed copper wire into the Ga. 27 tube and make several crimps with the tweezers. Insert the non-tapered end of the needle into the other end of the Ga. 27 tube and crimp together. Check the resulting connection for strength and electrical continuity.

(d) Prepare a small amount of Copper Bond™ epoxy for use by mixing the constituents together in a volumetric 50/50 mixture. Apply a small amount to the needle/wire junction, making sure that no metal components are exposed except for the very tip of the probe. The goal is to have the epoxy coating as thin as possible, and only have the tip of the needle exposed.

(e) Let the needle and wire air dry at room temperature for at least twelve hours.

(f) Insert the wire with needle into the probe casing, being careful not to break the wire/needle connection.

(g) Align the needle concentrically to the probe casing, leaving about 1/2 in. of the needle exposed past the casing.

(h) Prepare a small amount of Copper Bond™ epoxy for use by mixing the constituents together in a volumetric 50/50 mixture. Apply a small amount to fix and seal the needle to the probe end. Also apply a small amount to the other end of the probe to secure the thermocouple wire. Apply a small amount of the Stainless Steel Repair Kit epoxy to the stainless-steel tubing at the ninety degree bend.

(i) Let air dry at room temperature for one day.

(j) Using the Dremel (or fine 2000grit sand paper), sand the epoxy to make it smooth.

The finished probe should then be checked again for electrical continuity. The next section outlines the other hardware and software required for sampling and processing data from the single-sensor conductivity probe.

2.3. Hardware/Software for Data Acquisition

A list of the data acquisition hardware and software employed is shown as follows:

- Computer

  AMD @ 166MHz,

  32MB RAM, 2GB HD,

  Running Windows 95 ver 4.00.950B

- LabVIEW

  Version: 5.0.1

  Serial Number: G11X14939

- Data Acquisition Board

  Manufacturer: National Instruments

  Model Number: PCI-MIO-16E-4

  Part Number: 184002C-01

  Serial Number: ACAFAD

  Calibrated: October 22, 1998

- Shielded Connector Blocks

  Manufacturer: National Inst.

  Model Number: SCB-68

  Serial Number: ADC3A0

- Shielded 68 pin Cable, 1m

Manufacturer: National Inst.

Model Number: SH68

The impedance signals from the single-sensor conductivity probe are acquired by a National Instruments™ PCI-MIO-16E-4 data acquisition board. This data acquisition board can sample one channel up to 333,000 times per second with a resolution of 12 bits (1 part in 4096). The signals are sampled for 60 seconds at 10 kHz. for each probe position. It should be noted that the sampling time and frequency are unique to each application. For example, a longer sampling time will increase the accuracy of the measurement, statistically. The sampling frequency should then be determined by the Nydquist approach. For the data sampled in this thesis, a sampling time of 60 seconds and a sampling frequency of 10 khz. is more than adequate. An AMD-166 MHz processor with 32MB RAM and a 2GB HD is used for the data acquisition computer. Windows 95 (version 4.00.950B) is used as the operating system to run LabVIEW version 5.0.1.

To provide a potential between the probe tip and the probe casing, a 6 V, 10 Ah sealed lead-acid direct-current (DC) battery is used as the power source. In order to decrease the current flow in the water medium, mega-ohm resistors are used as shown below. A resistivity box was constructed with two separate circuits (the other to be used later in a double-sensor probe) containing multiple mega-ohm resistors in series with a selecting switch. If signal degradation is apparent from tip corrosion after many hours of use, the resistance of the circuit may be decreased to compensate. The circuit along with the resistivity box used is shown in Figure 5.

Figure 5 below shows the wiring schematic for the single-sensor probe. Notice that Tip Two (not shown) in the resistivity box is not used for the single-sensor conductivity probe. Also, it is very important to have a good ground on the computer to help reduce the noise in the system. The data collection procedure will now be addressed.

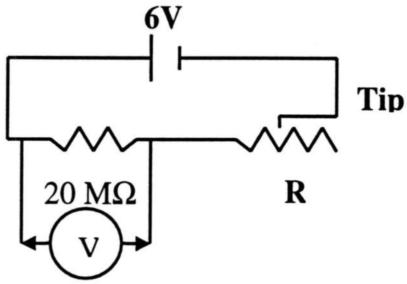

Figure 5 (a) Circuit design.

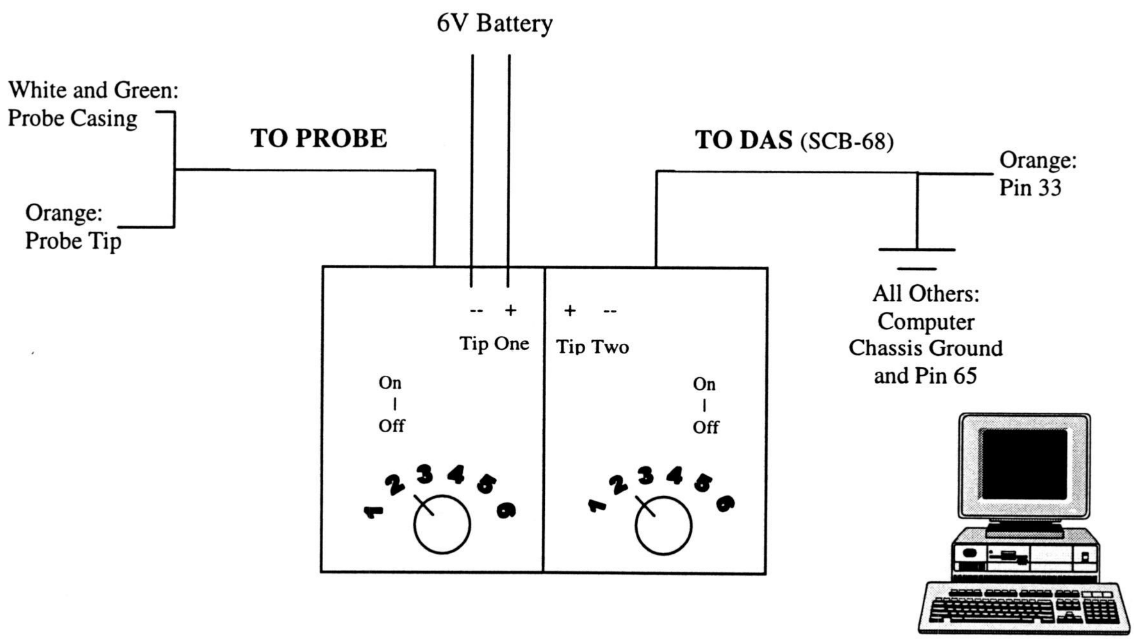

(b) Resistivity box.

Figure 5. (a) Circuit design and (b) resistivity box used.

2.4. Procedure for Data Collection

The following procedure is commonly employed for void fraction measurement in vertical air-water systems at the OSU Advanced Thermal Hydraulic Research Laboratory (ATHRL) [15].

- Warm up electronic equipment for a minimum of 5 minutes prior to taking data.
- After a change is made in the test conditions, let the system stabilize for at least one minute before collecting data.
- Ensure the conductivity probe is aligned vertically to the flow.

  Data Acquisition Startup:
- Turn on computer if not already running. Make sure all programs are closed, then open "LabVIEW" [16].
- Open "NI-DAQ Configuration Utility" program:
- Ensure in "DAQ Devices" folder that "Device #1: PCI-MIO-16E-4" is listed.
- Highlight above "Device" and click on button "Configure."
- Ensure device is listed as "#1" in "System" folder.
- In "AI" folder (Analog Input), ensure Polarity is set from "0 - +10V."
- Ensure that the Mode is "Referenced Single Ended."
- Ensure "AO" folder is empty.
- "OPC" folder should have the "AI Recalibration Period" disabled.
- In the "Accessory" folder, the "SCB-68" option should be highlighted.
- After everything is confirmed, save the file and then exit.
- Open "DAQ Channel Wizard" program:
- Ensure "Scales" folder is empty.

- Ensure that the "Devices" folder has the PCI-MIO-16E-4 and SCB-68 listed.
- In "Channels" folder, one channel (One) should be configured by highlighting that channel and clicking on the "Edit" button.

> NOTE:
>
> It is important to note the correct location for pin # on the channel that is being measured. That is also why the "NI-DAQ Configuration Utility" program is run first in order to specify the style connector block used. The pin # will vary depending on connector block used as well as the "Input Mode" specified. If changes are made, click on button "Apply" and then "Return." Finally, click on button "Save" at the bottom and then "Exit." This will take you back to LabVIEW.

- Ensure that the "Description" matches the probe configuration: the "1) Physical Quantity" is correct as well as the "2) Sensor" information. "3) DAQ Hardware" lists the Devices used and the location where the Analog Input wire for that channel should be placed in the connector block.
- Open a VI (Virtual Instrument) in the directory " c:\Cond Probe\condprobe2.vi "

> NOTE:
>
> This program launches a Panel as well as a Diagram interface. Please consult the LabVIEW manual for more information about LabVIEW programs and G-programming. Both windows can be displayed at the same time by re-sizing them.

The Panel and Diagram interface are shown in Figures 6 and 7 for this condprobe2.vi program.

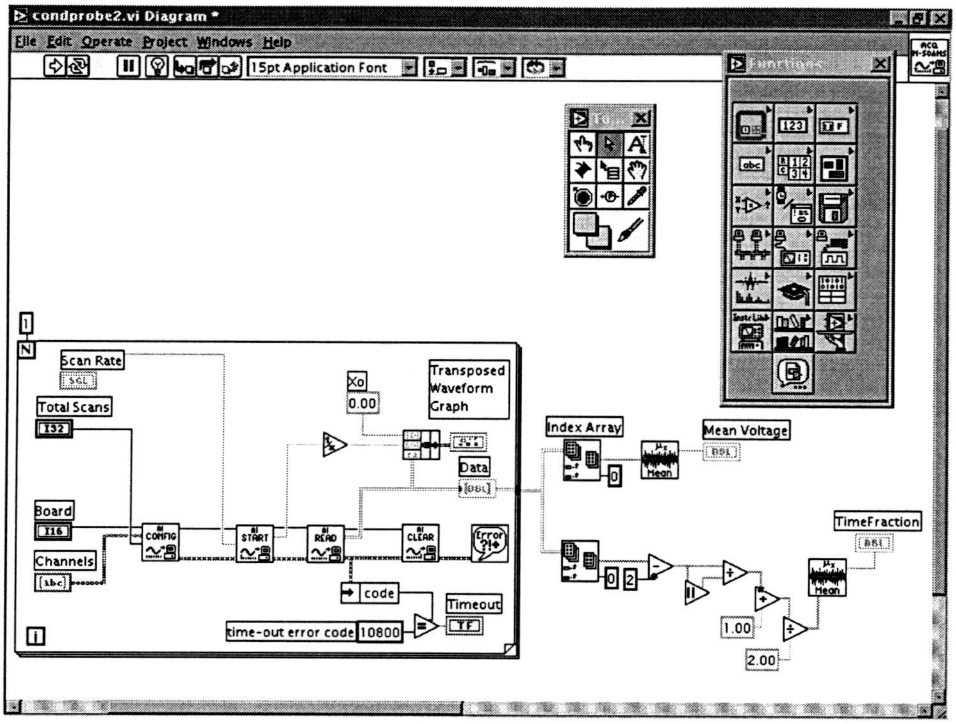

Figure 6. Labview "Panel."

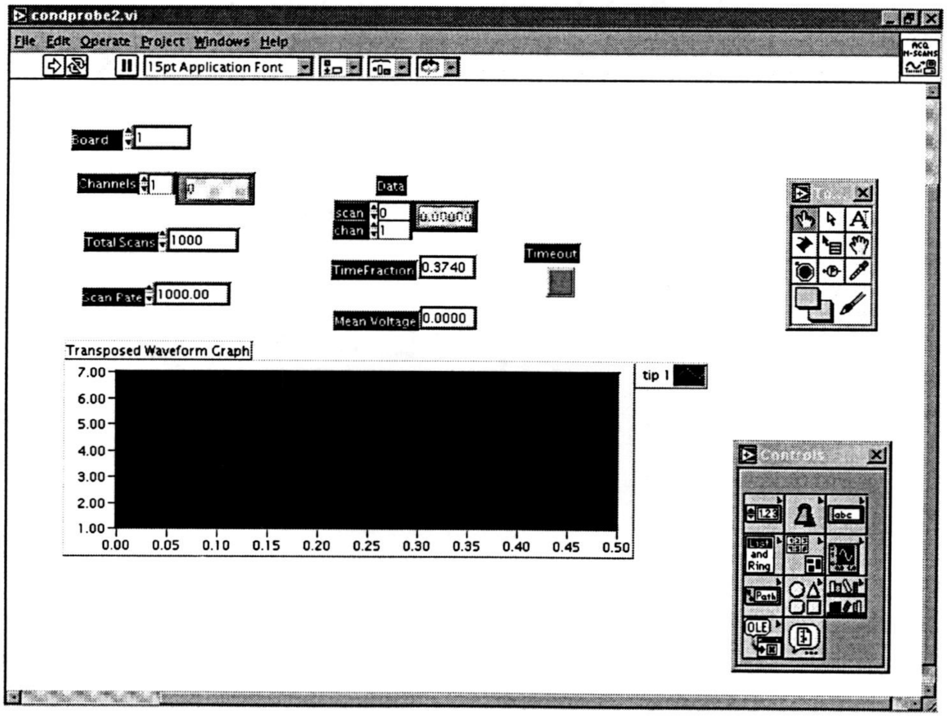

Figure 7. Labview signal processing "diagram."

- Ensure at "Panel" interface "Board #" is 1.
- Ensure that "Channels # " is "1" and "1" is typed in the right box as well.

NOTE:

For example, this means one channel will be read and it is called channel "1" (as designated in the "DAQ Channel Wizard" program).

- Set "Total Scans" to "500,000."
- Set "Scan Rate" to "10,000" Hz.
- Ensure that the Transposed Waveform Graph at the bottom of the window has the vertical scale from "0 to 10" (V). The horizontal scale should be from "0 to 0.20" (seconds).
- Go to the "Diagram" window. Look for the text box "Change The Value Above Only." Click in the box above the text box and change this numerical value to "0." This sets the lower limit cut-off for the time fraction calculations as described earlier.
- Ensure probe is aligned vertically to the flow.
- Return to "Panel" display.
- Click on "Operate" at the top of the window.
- Click on "Run."

NOTE:

A voltage readout vs. time should appear on the graph after the program finishes collecting and processing the data. 10,000 Hz should be sufficient for the bubble velocity encountered in this test. Look at the graph where the minimum voltage read is. Manipulate the vertical axis scale to see it better.

- Find where the minimum voltage read is, or the "baseline voltage." Add 0.05 volts to this "baseline."
- Change the minimum vertical axis scale to the "baseline + 0.05 V" value.

NOTE:
The purpose is to display only the region where a "bubble is occupying the probe tip." Anything less than this voltage will be interpreted as a liquid phase. The baseline voltage should not be displayed.

- In the "Diagram" window, change the previous numerical box # to this baseline voltage plus 0.05 volts (as described above).
- Click on "Operate."
- Click on "Run" again to collect data. Record the Time Fraction data in the Panel interface. Multiply this value by 100 to obtain the local time-averaged void fraction in percent.
- Keep checking the baseline voltage since drifts may occur with different void fractions and change as necessary.

In conclusion, a list of typical equipment used and the data acquisition procedure for a single-sensor conductivity probe was presented. The time fraction, or void fraction, is at one position (probe tip position) however. The probe tip may be moved accordingly in the test section to obtain a void fraction profile. This profile may then be properly area-averaged depending on the geometry of the test section.

3. EXPERIMENTAL COMPARISON OF SINGLE-SENSOR PROBE DATA TO OTHER MEASUREMENT TECHNIQUES AND CORRELATIONS

In this chapter, an experimental effort is described in which the void fraction results from the single-sensor probe are compared to data from a capacitance probe, visual data, and two correlations [17].

The two-phase fluid mixture level in the reactor vessel is one of the most important parameters for the assessment of reactor safety. Therefore, it is essential that the techniques used to measure or calculate the two-phase fluid mixture level are accurate. For this purpose, a test facility was designed and constructed, which has a vertical, cylindrical, transparent test section having an inner diameter of 15.2 cm. It includes a lower plenum mixing chamber with separate air and water inlets. The parameters measured included air flow rate, collapsed liquid level, level swell and local void fraction. The collapsed liquid level was measured using a differential pressure cell. The fluid mixture level was measured using a fixed scale for visual indication and a Drexelbrook Level Transmitter™ capacitance probe. A traversing, single-sensor, conductivity probe was used to obtain an area-averaged measurement of the local void fraction. Comparisons were made for different measurement techniques used in the test facility. Also, the results were employed to assess two commonly used correlations for the prediction of void fraction in a pool boiling system.

3.1. Test Facility and Instrumentation

3.1.1. Test Facility

The test facility, shown in Figure 8, was designed to simulate level swell recordings as observed within Oregon State University's (OSU) Advanced Plant Experiment (APEX). The OSU APEX test facility is a one-fourth height, one-half time scale, reduced pressure integral systems model of the Westinghouse AP600 Pressurized Water Reactor. One of the objectives of the AP600 research at OSU was to obtain APEX data to validate Westinghouse and NRC thermal-hydraulic computer codes.

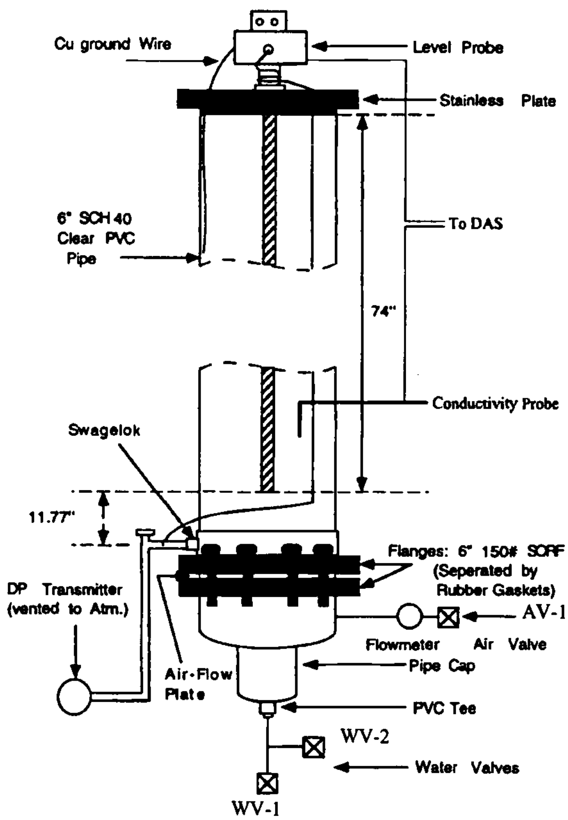

Figure 8. Schematic of the test facility.

As shown in Figure 8, the capacitance probe sits inside the 15.2 cm. ID clear PVC pipe to allow visual confirmation of the level swell using a fixed scale. Visual level swell was estimated as an average height of the chaotic, turbulent mixture from the base by using a tape measurer. A steel plate flange at the top of the pipe supports the weight of the probe. Two more flanges at the bottom of the pipe were used to confine an air-flow plate, and support a pipe cap. The pipe cap is the mixing section, and is filled with air and water. A grounded copper wire connects the capacitance probe to the inner wall surface of the PVC piping. This procedure is necessary for obtaining reliable data, since the capacitance probe would normally be placed inside a metal column (such as the APEX reactor vessel). Two single-sensor conductivity probe ports were drilled in the side of the test section, at elevations 54.26 cm. and 92.36 cm. above the air-flow plate. The bottom pressure tap for the Rosemount™ Differential Pressure (DP) Transmitter was placed just above the inlet to the test section to measure the collapsed liquid level during operations.

3.1.2. Instrumentation

Two state-of-the-art instruments were employed in this test: a Drexelbrook™ Universal II Series Capacitance Probe [18] and a single-sensor conductivity probe [15]. Both of these are described below.

3.1.2.1. Capacitance Probe

The capacitance probe measures an average liquid level height within a confined system. For this experiment, the system boundary is the PVC tube. The tube walls and the probe act as capacitance plates for the system. In between, the liquid level swell acts as a dielectric, adjusting the output of the device. In conjunction with this, the probe's recorded dielectric constant serves as a calibration level check. The level transmitter can provide both point level and continuous level measurement and will perform in a variety of liquids and temperatures. Its measurements are independent of the liquid's changes in density, chemical composition, and electrical properties.

To monitor and store experimental data from both the capacitance probe and the DP transmitter, a Data Acquisition System (DAS) was installed. The instrument that provided this function was a FLUKE Data Bucket that had been calibrated according to the OSU Maintenance Manual [18]. The Data Bucket collected data from two separate channels. Channel 1 corresponded to the DP Transmitter, and Channel 2 to the capacitance probe. A 2 MB card, specifically designed for the Data Bucket, recorded data from both channels once every second. A Westcon™ digital panel meter provided a secondary method for local online viewing of measurements from the DP Transmitter and capacitance probe. Details of the official test procedure can be found in [18].

The principle of measurement of a volume-averaged void fraction using the level probe is relatively simple. If the reading of the mixture level is H_m and the collapsed liquid level measured using a differential pressure cell is H_c, the volume averaged void fraction in the test section should be (since volume is directly proportional to height for the constant cross-sectional area of the test section):

$$<\alpha>=\frac{H_m - H_c}{H_m} \tag{3.1}$$

The mixture level can also be measured through visual observation using a fixed length scale on the side of the transparent test section.

3.1.2.2. Conductivity Probe

A single-sensor conductivity probe was made and installed to obtain the time-averaged void fraction at the tip of the probe. The probe design was shown previously in Figure 1.

The impedance signals from the probe are acquired by a National Instruments™ PCI-MIO-16E-4 data acquisition board. The signals were sampled for 40 seconds at 10 kHz for each probe position. An AMD-166 MHz processor with 32 MB RAM and a 2GB HD was used for the data acquisition computer. Windows 95 (version 4.00.950B) was used as the operating system to run LabVIEW version 5.0.1. A simple algorithm was used to determine the appropriate phase from the impedance signal. The time fraction of the gas phase was then calculated by the equation below:

$$\overline{\alpha}^{t} \equiv \frac{\sum \Delta t_{ki}}{T} \tag{3.2}$$

where T is the total time measured, and Δt_{ki} is the time occupied by the gas phase. Symmetry was assumed for the test section. Therefore, the probe was positioned at radial locations corresponding to r/R = 0, 0.167, 0.333, 0.5, 0.667, and 0.833. The void fraction , by definition, is zero at the wall. The local time-averaged void fractions obtained at the radial positions above were then area-averaged:

$$\overline{\alpha}^{A} \equiv \frac{\sum A_{ki}}{A} = \frac{1}{A}\int \overline{\alpha}^{t} dA \tag{3.3}$$

This yielded the area-averaged, time-averaged void fraction at an axial location. Details of the procedure used in collecting this data were found previously in Chapter 2. Data were collected at two axial locations in the test section: one at a collapsed liquid level of 48.26 cm., and another at a collapsed liquid level of 86.36 cm. These locations corresponded to the data obtained from the capacitance probe.

Comparisons were made with the volume-averaged measurements using level probe and visual observation, based on an assumption that the area-averaged void fraction does not change along the flow direction, which is valid for flow in a relatively short test section without phase change. Bubble expansion effect was neglected because the volume change is within 1% for this short test section height.

3.2. Pool Boiling Correlations

This section presents two correlations used in predicting the void fraction within a vertical saturated pool boiling system. The correlations are the result of a number of experiments using a variety of vessel hydraulic diameters.

3.2.1. Kataoka and Ishii

The Kataoka and Ishii pool boiling void fraction correlation was developed from the drift flux model [19]. Their final equation took the following form:

$$<\alpha>=\frac{<j_g>}{C_o<j_g>+<<V_{gj}>>} \tag{3.4}$$

where $<j_g>$ is the superficial velocity. For a round tube, the distribution parameter C_o is defined as:

$$C_o=1.2-0.2\sqrt{(\rho_g/\rho_f)} \tag{3.5}$$

The void-weighted, area-averaged, drift velocity ($<<V_{gj}>>$) in Equation (3.4), is obtained from the following relation:

$$<< V_{gj} >> = V_{gj}^{+}\left(\frac{\sigma g \Delta\rho}{\rho^{2}_{f}}\right)^{1/4} \tag{3.6}$$

In this equation, the dimensionless velocity, V_{gj}^{+}, is defined as:

$$V_{gj}^{+} = 0.92(\rho_g / \rho_f)^{-0.157} \quad \text{for } D_H^{*} \geq 30 \tag{3.7}$$

The dimensionless hydraulic diameter, D_H^{*}, is defined as follows:

$$D_H^{*} = \frac{D}{\sqrt{\frac{\sigma}{g\Delta\rho}}} \tag{3.8}$$

$D_H^{'}$ was determined to be 56.2 for the test section.

3.2.2. Boesmans and Berghmans

The Boesmans and Berghmans [20] void fraction correlation for a pool boiling system is given by:

$$\frac{1}{<\alpha>} = C_o + F_{ci}\frac{C_1}{Fr} \tag{3.9}$$

Equation (3.9) is valid only when $D_H^{*} > 30$ and $D/H \leq 0.2$ to ensure that the correlation is excluded from slug flow and short tubes. The experimental values are within both of these ranges. The distribution parameter, C_o, and velocity coefficient, C_1, depend upon the flow patterns. For this experiment the following equations were used for churn-turbulent flow:

$$C_o = 1.2 \tag{3.10}$$

$$C_1 = 1.373 + 0.177\left(\rho_g / \rho_f\right)^{-0.25} \tag{3.11}$$

The liquid circulation factor in Equation (3.9), (F_{ci}), is typically treated as a constant value of 2. The Froude number (Fr) is derived from the drift flux model and takes the following form:

$$Fr = < j_g > \left(\frac{\rho^2{}_f}{\sigma g \Delta\rho} \right)^{1/4} \tag{3.12}$$

3.3. Results

Two test series were run. The parameters varied were the initial collapsed liquid level and the air flow rate. Two initial collapsed water level heights were implemented: a collapsed level of 48.26 cm. and a collapsed level of 86.36 cm. The collapsed liquid levels were measured by using a differential pressure cell and also visually by using an external scale. For each of these tests, air was injected at the bottom of the test section through a mixing plenum to obtain gas superficial velocities ranging from 0.088 to 0.285 m/sec. A traversing single-sensor conductivity probe was employed to measure the local, time-averaged void fraction, which was then area-averaged for comparisons. Table 1 presents the test matrix. The measured void fractions, along with two appropriate correlations, were then plotted as a function of the superficial gas velocity for the two tests.

TABLE 1. Test Series and Matrix

Test Series	Collapsed Liquid Level (cm)	Air Flow Rates (m^3/sec)
1	48.26	1.57, 1.97, 2.36, 2.75, 3.15, 3.54, 3.93, 4.33, 4.72, 5.11
2	86.36	1.57, 1.97, 2.36, 2.75, 3.15, 3.54, 3.93, 4.33, 4.72, 5.11

The measured level swell from the capacitance probe was compared to the level swell determined visually for the two initial collapsed water levels. These comparisons are shown in Figures 9 and 10.

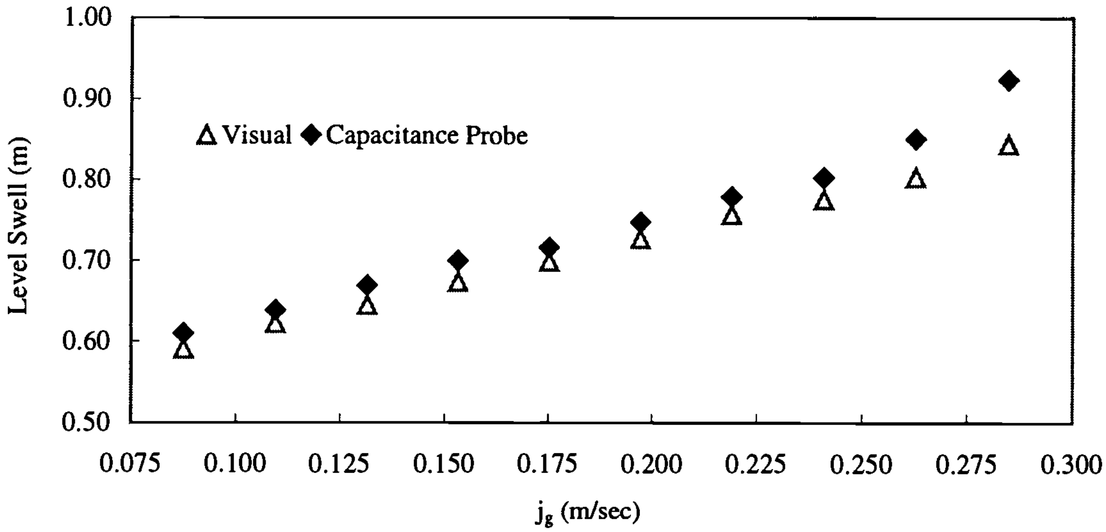

Figure 9. Plot of level swell at 48.26 cm. collapsed water level.

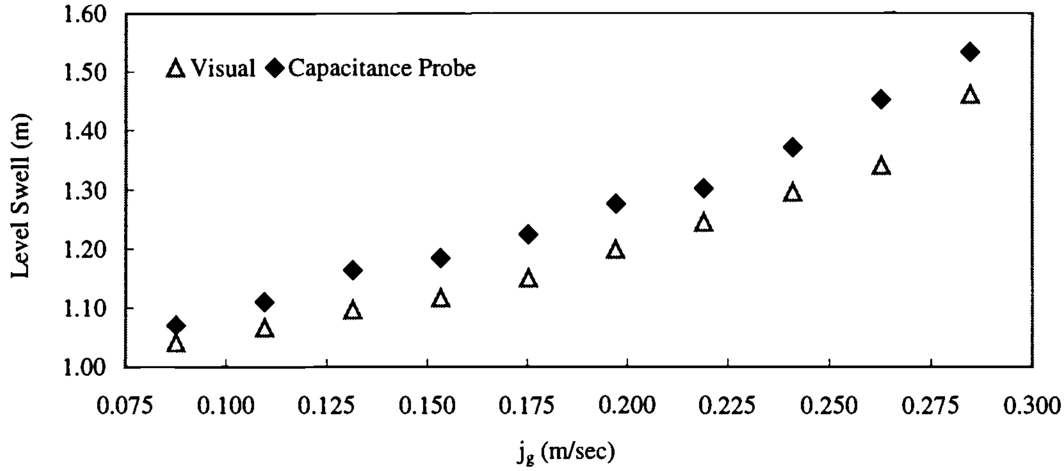

Figure 10. Plot of level swell at 86.36 cm. collapsed water level.

The level swell measurements were then used to calculate volume-averaged void fractions. Void fraction as a function of the superficial gas velocity is plotted in Figures 11 and 12 for the various instruments and correlations.

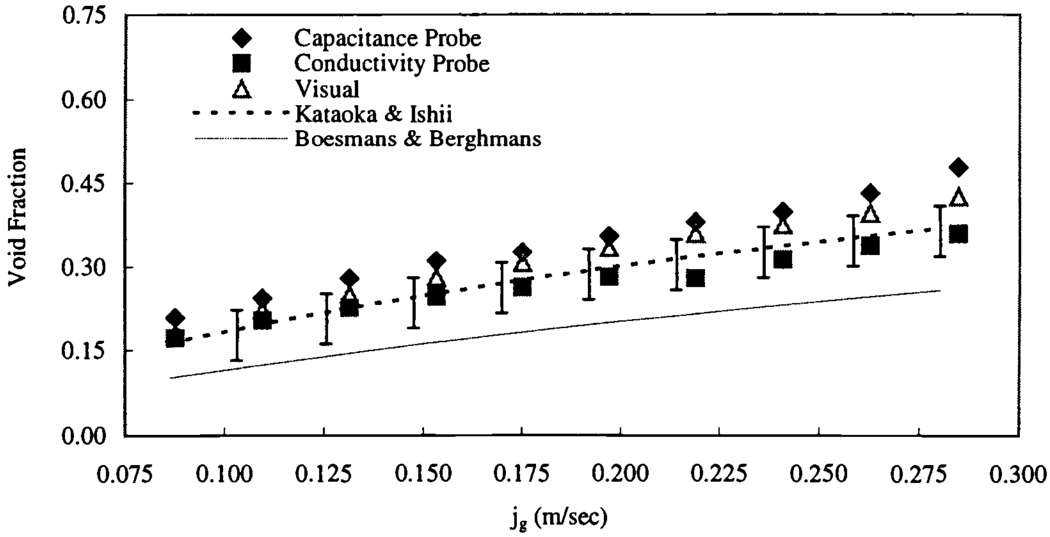

Figure 11. Plot of void fractions at 48.26 cm. collapsed water level.

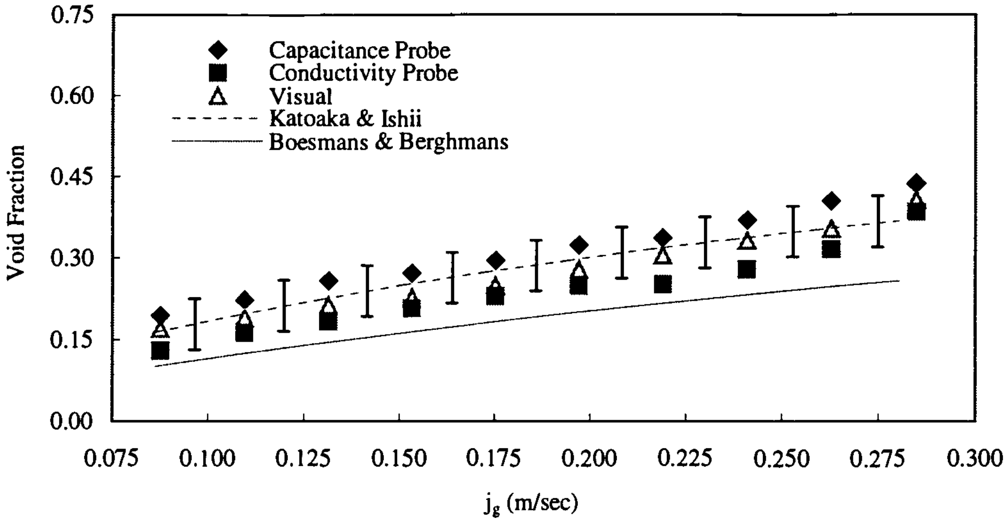

Figure 12. Plot of void fractions at 86.36 cm. collapsed water level.

As shown previously in Figures 11 and 12, the visual measurements and Katoaka and Ishii's correlation agree quite well, with a relative discrepancy of ± 9%. The correlation by Boesmans and Berghmans predicts a slightly lower void fraction as compared to the visual measurements. Both correlations appear to level off as j_g increases, whereas the capacitance probe and visual measurements remain linear. The conductivity probe measurements seem to decrease around a j_g of 0.2 m/sec and then increase again around a j_g of 0.28 m/sec. While the capacitance probe measures a slightly higher void fraction (compared to the visual measurements), the conductivity probe agrees very well with the visual data up to a j_g up to 0.225 m/sec. A radial profile of the void fraction as obtained with the conductivity probe is shown in Figure 13 for a spectrum of superficial gas velocities. As j_g increases, the local void fraction in the center of the test section increases more than near the test section wall, as expected.

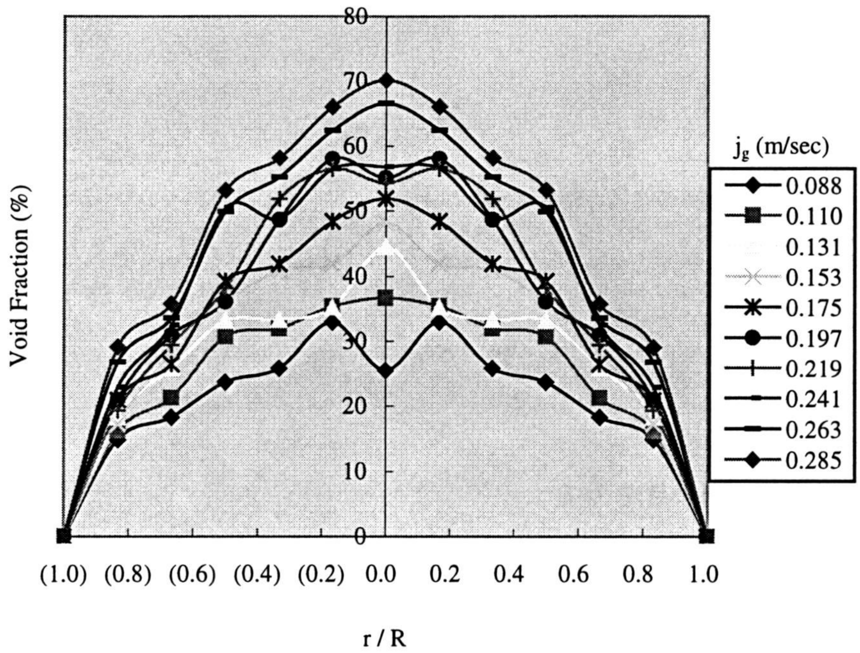

Figure 13. Void fraction radial profile as measured with the conductivity probe at 48.26 cm. collapsed water level.

3.4. Conclusions

Level swell, as measured visually within the test facility, can be accurately predicted by Kataoka and Ishii's correlation within approximately 9% void fraction, while Boesmans and Berghmans correlation underestimates void fraction substantially. The Drexelbrook capacitance probe overestimates the level swell when compared with visual data by approximately 15%, while the conductivity probe underestimates the level swell compared to the visual data by approximately 10%. The conductivity probe void fraction measurements lie within the uncertainty in Kataoka and Ishii's correlation.

4. DESIGN CRITERIA FOR A DOUBLE-SENSOR CONDUCTIVITY PROBE

The design criteria for a double-sensor conductivity probe is determined in this chapter from a literature review [21]. The design and manufacture of a double-sensor probe differs from a single-sensor needle-type probe (Chapter 2) only in the addition of another accupunctual needle and the spacing of this needle tip in relation to the first needle tip.

In order to accurately measure a bubbles interfacial velocity in two-phase flow and relate this to its interfacial area concentration, a certain number of restrictions are placed on the flow conditions as well as the double-sensor probe design. First, the fundamental principle of how a double-sensor probe measures the velocity of a bubble is explained. Next, the measured bubble velocity from the double-sensor probe is statistically related to the actual bubble velocity, and then in turn, substituted into a formula that yields the interfacial area of the bubble. This kind of double-sensor probe can provide both local time-averaged void fraction as well as local time-averaged interface velocity and interfacial area – all of the key parameters needed to evaluate the interfacial area concentration transport equation [22, 23, 24]. Therefore, although experimental results from the double-sensor probe was not a thesis task, the principle, design criteria and manufacture procedure (similar to single-sensor probes) are summarized and presented in this thesis as a guide for further investigations.

4.1. Principles of Measuring Bubble Velocity

If the distance between two probe tips is known, then the measured velocity of a bubble can be determined from the time difference as it passes from the first tip to the second (determined by the voltage vs. time plots for the two sensors). There are a few important assumptions that need to be stated before the actual bubble velocity can be assumed equal to the measured bubble velocity. First, it is assumed that the probe is aligned parallel to the mean bubbly flow. Secondly, the probe tips do not alter the bubble trajectory or the bubble does not change course as the bubble leading surface moves through the two probe tips. Lastly, the bubbles are spherical and do not distort as they pass through the probe tips. If these criteria are met, then the measurable bubble velocity is $V_m = \Delta s/\Delta t$, which is equal to the actual bubble velocity, V. These conditions are difficult to meet in real-world applications, and therefore analyses have been performed below to determine the effects of non-ideal conditions imposed on the measured bubble velocity [21, 25].

There are also problems on how to account for "missing bubbles." For example, a bubble may touch the tip of one sensor, but miss the other sensor. Or, the bubble may be moving almost completely sideways to the probe so that from the probe signals, the measured velocity is very large. One other factor to account for in actual measurements is the fact that the bubble velocity fluctuates with lateral components as it passes through the two sensors. Both of these factors are related to the probe spacing, Δs. These three variables, missing bubble phenomena, velocity fluctuation, and probe spacing, are taken into account when defining a calibration factor that relates the true bubble velocity to the measured bubble velocity. This calibration factor is discussed below.

4.2. Theoretical Calibration Factor

The theoretical calibration factor is defined as the ratio between the actual mean bubble velocity, $\overline{V}$ and the mean measurable bubble velocity, $\overline{V}_m$:

$$f = \frac{\overline{V}}{\overline{V}_m} \tag{4.1}$$

In developing this theoretical calibration factor, the mean bubble velocity was rigorously related to the mean measurable velocity by defining appropriate probability distribution functions. For an in-depth investigation, please refer to [21]. The three variables listed previously, missing bubble phenomena, isotropic velocity fluctuation, and probe spacing, are taken into account for the calibration factor below.

$$f_{total} = 2 + \left(\frac{V_b'}{\overline{V}_b} \right)^{2.25}, \text{ for } \Delta s = 0.36D \sim 0.86D \text{ and } \frac{V_b'}{\overline{V}_b} = 0 \sim 0.5 \tag{4.2}$$

Using a Monte Carlo approach provided the necessary sample size for a given statistical uncertainty for Equation (4.2). The true bubble velocity will have a statistical error of ± 8.5 % for a sample size of approximately 1,000 bubbles using (4.2) [21]. In the above calibration factor, it is assumed that the lateral bubble motions are driven mainly by turbulent eddies in the flow medium, and that the motions of these eddies are approximately isotropic with a first-order accuracy. This may not be valid for entrance regions or near a wall [21, 22].

A study [21] suggested that even if the bubble does not have an isotropic velocity fluctuation and instead the axial velocity fluctuation is twice that of the lateral velocity fluctuation, then the calibration factor given in Equation (4.2) may still be used with the same uncertainty if the probe spacing is changed from 0.5 to 1 times the mean bubble diameter. The above analysis still assumes that the bubble does not alter its trajectory after it penetrates the first probe tip.

4.3. Interfacial Area Calculation

The local interfacial area concentration is given by Ishii [8] as:

$$\overline{a_i} = \frac{1}{\Delta T} \sum_j \left(\frac{1}{|\vec{v}_i \cdot \vec{n}_i|} \right)_j \tag{4.3}$$

Where j denotes the j-th interface passing through a point during the time interval ΔT. The vectors $\vec{v}_i$ and $\vec{n}_i$ denote the local bubble interface velocity and the surface normal vector, respectively (hence the assumption that $|\vec{v}_i \cdot \vec{n}_i|$ remains constant as the bubble passes from the first tip to the second). Neglecting bubble velocity fluctuations as well as probe spacing and missing bubble phenomena, (4.3) was simplified to the following:

$$\overline{a_i} = f \frac{2N_b}{\Delta T} \left(\frac{1}{\overline{v}_m} \right), \text{ where } v_m = \frac{\Delta s}{\Delta t} \tag{4.4}$$

In Equation (4.4), the calibration factor, f was equal to the constant value of 2.

An alternate, more accurate approach using the calibration factor defined in (4.2) and accounting for the missing bubble phenomena [21] yields a revised formula for the local interfacial area concentration:

$$\overline{a}_i = \left(\frac{2N_b}{\Delta s \Delta T} \right) \left[2 + \left(\frac{V_b'}{\overline{\overline{V}}_b} \right)^{2.25} \right] \left[\frac{\sum_j (\Delta t_j)}{N_b - N_{miss}} \right], \text{ for } \Delta s = 0.36D \sim 0.86D \text{ and } \frac{V_b'}{\overline{\overline{V}}_b} = 0 \sim 0.5 \tag{4.5}$$

$V_b^{'} / \overline{Vb}$ is defined as the relative bubble velocity fluctuation. Equation (4.5) also assumes that the bubble velocity fluctuation is isotropic. N_b and N_{miss} are the total number of bubbles and the missing number of bubbles, respectively, during time ΔT.

In conclusion, Equation (4.5) may be used to calculate the interfacial area concentration to within $\pm 8.5\%$ for a sample size of approximately 1,000 bubbles. Wu et al. [21, 25] accounted for many potential factors that relate the measurable bubble velocity to the real bubble velocity and determined that given the assumptions listed above, the interfacial area concentration can be measured reasonably accurately using the double-sensor probe technique. The next chapter discusses the development and application of a probe in measuring area-averaged void fraction, the half-ring probe.

5. HALF-RING TYPE PROBE

The purpose of this study is to design an instrument capable of measuring time and area-averaged (over a circle) void fraction in a two-phase, air/water system. The data from this probe will be used in development of new liquid entrainment models in reactor hot legs [26]. One instrument theoretically capable of accomplishing this is the half-ring conductivity probe. This intrusive probe consists of two stainless steel (SS) wires, with the wires laid across from each other in a half-ring geometry. A half-ring probe is shown below in Figure 14. An alternating current (AC) circuit is proposed to minimize corrosion of the wires and to also reduce the voltage drift due to ions in the water migrating. Design and testing of a half-ring conductivity probe has been completed for a stagnant two-phase system in a 6 in. ID vertical and horizontal pipe. Preliminary data from the vertical pipe experiment and a cross-calibration with a single-sensor conductivity probe is outlined below.

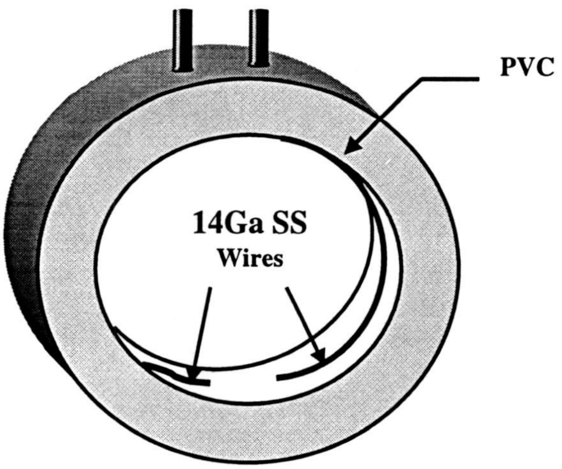

Figure 14. Half-ring conductivity probe.

5.1. Necessity of Half-Ring Probe

The motivation of this probe configuration is to design an instrument to collect data in support of a new liquid entrainment onset model [26]. Oregon State University (OSU) has a contract with the Nuclear Regulatory Commission (NRC) to study phase separation in tees. Accurate modeling of phase separation is crucial to current reactor safety codes [27, 28]. In an accident situation, automatic depressurization systems (ADS) are used to depressurize the reactor such that a low-pressure injection system may be used, or gravity-driven natural circulation may occur. Previous studies have focused on phase separation in horizontal ducts (the hot legs) with a vertical tee branch simulating the break. The studies used stratified flow conditions, and were used to develop models in the INEEL RELAP5 code. However, in recent NRC tests conducted at the OSU Advanced Plant EXperiment (APEX), the liquid entrainment predicted by RELAP5 was lower than experimental data. This is not a conservative model, and needed to be further evaluated. A new Liquid Entrainment Separate-Effects Test (LESET) facility has been constructed at OSU simulating a prototypic reactor hot leg with a break in an ADS tee junction. Preliminary visual observations suggest that the flow is not stratified, and that it is generally bubbly or intermittent flow, shown in Figure 15.

The current correlations used in nuclear reactor safety analysis programs are dependent on the liquid level in the hot leg, while it has been proposed that they be based on the void fraction in the hot leg [26]. Current instruments that can measure an instantaneous (relatively speaking ~1 msec.) area-averaged void fraction include magnetic resonance imaging (MRI), a one-shot gamma densitometer, and acoustic bubble imaging. The MRI system is too expensive, and the acoustic bubble imaging technique is still under development. The one-shot, sixteen channel gamma densitometer is currently under development at OSU and would be the ideal instrument to use in the LESET experiments. However, it requires a radioactive source, and only a few specially trained personnel are qualified to use this. Therefore, the laboratory would be off-limits to many others during testing. It is also a bulky, expensive system to use and manipulate. Therefore, a half-ring conductivity probe is proposed to work in conjunction with the gamma densitometer. The gamma densitometer will be used to calibrate the half-ring probe to measure area-averaged void fraction for varying flow regimes in the LESET hot leg inlet. However, due to the gamma densitometer development time constraints, the cross-calibration with this system was not accomplished, and instead, the area-averaged single-sensor conductivity probe results were used.

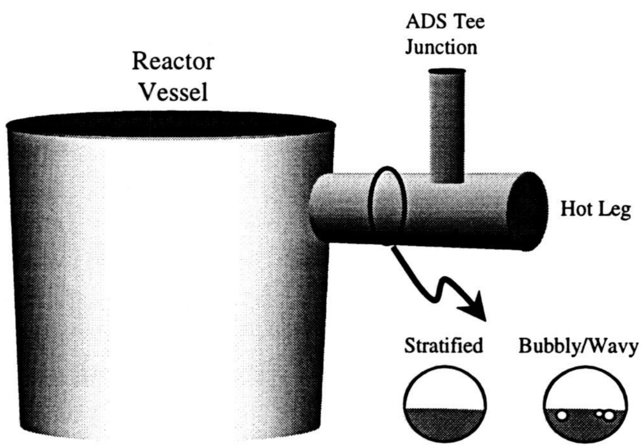

Figure 15. Separate-effects test.

The area-averaged single-sensor conductivity probe results from Chapter 3 were used as a preliminary cross-calibration with the half-ring probe. It should be noted that the orientation of the pipe in the LESET experiment is horizontal, while the orientation of the pipe in the other experiment was vertical. For the cross-calibration, the test section described in Chapter 3 was modified by cutting the 6 in. ID pipe and inserting flanges so that the half-ring probe could be inserted at identical measurement locations to the single-sensor conductivity probe. This enabled a consistent cross-calibration between the two instruments to be performed. For insertion into the LESET experiment, the half-ring probe will need to be cross-calibrated again with either the gamma densitometer or area-averaged data from the single-sensor probe in this particular horizontal pipe orientation.

5.2. Half-Ring Probe Theory of Operation

After consultation with a number of physics professors at OSU, a detailed analysis of the theory of operation behind this half-ring probe was discouraged due to the complex geometry of the two interacting electrodes. A mathematical formulation for this electric-field interaction should be performed before the probe is widely applied. A rudimentary attempt at describing the half-ring probe operation follows.

Ohm's law relates the time rate of charge passage, I, through a conductor to the applied voltage, V, and the resistance, R, by the following equation:

$$V = IR \tag{5.1}$$

The value of the resistance, R, is influenced by the configuration of the conductors, and is related to the resistivity, ρ, by:

$$\rho = \frac{RA}{l} \tag{5.2}$$

Here, l is the distance between the two points where the voltage is measured, and A is the cross-sectional area perpendicular to the direction of the current. The conductivity is just the inverse of reactivity.

By measuring the changing conductivity of a two-phase air/water mixture, the void fraction may be theoretically determined. The current drawn by the probe (driven with a constant amplitude AC voltage source) is related to the area-averaged void fraction.

5.3. Design of the Half-Ring Conductivity Probe

5.3.1. Materials and Machining

The OSU LESET facility has a 6 in. ID at the hot leg inlet. Therefore, the half-ring probe was designed with the same inner diameter such that it will fit between the hot leg and reactor vessel flanges. The probe was constructed from an electrically insulated material that was inexpensive and easy to machine (gray polyvinylchloride, or PVC). One 6 inch inner diameter probe that is 2 in. thick may be machined from approximately $40 of gray PVC. The probe was machined with two small rings in the inner diameter periphery such that two conducting stainless steel wires could be inlaid. A drawing of the OSU half-ring probe is shown in Figure 16.

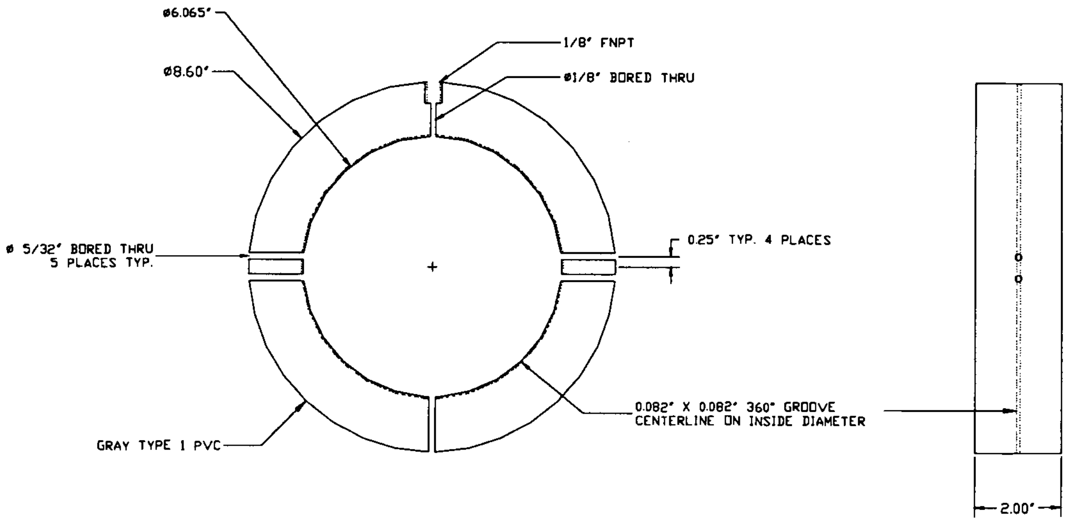

Figure 16. Half-ring conductivity probe.

5.3.2. Power Supply

An Alternating Current (AC) circuit had been proposed instead of the conventional Direct Current (DC) power supply. One benefit from the AC circuit is reduced corrosion of the wires. Also since tap water will be used in the experiments, the AC eliminates ion migration. The ion migration will tend to increase voltage over time since the ions in the water migrate to their respective oppositely charged electrodes over time. This time is on the order of milli-seconds, and becomes significant for long sampling times. The base circuit used is from the OSU Oceanography Department [29]. Mr. Steve Smith has modified this design slightly and etched a circuit board for this circuit instead of using a breadboard. The result is a more professional quality and lower noise in the circuit. The circuit is powered with a common +/ 15 V power supply and relies on a constant voltage source (with a feedback circuit) across the probe electrodes to measure the current draw.

This current draw is inversely proportional to resistance from Ohm's law. Similarly, the resistance is directly proportional to the area-averaged void fraction between the probe electrodes. For example, if the ring is initially flooded with water, the voltage output from the probe circuitry can be adjusted to yield a maximum of 10 V. If this water is completely displaced with air, the conducting medium (water) is no longer there, so the current draw from the probe will be zero. This can also be adjusted to yield a minimum of 0 V. An oscillator outputs a constant frequency 10 kHz. sine wave. A simplified diagram of the fundamental circuit design is shown in Figure 17. A waterproof NEMA-4 box contains the power supply and circuit board. Shielded cables are used to reduce noise in the system, and care is taken to isolate the power cables from the instrumentation cables.

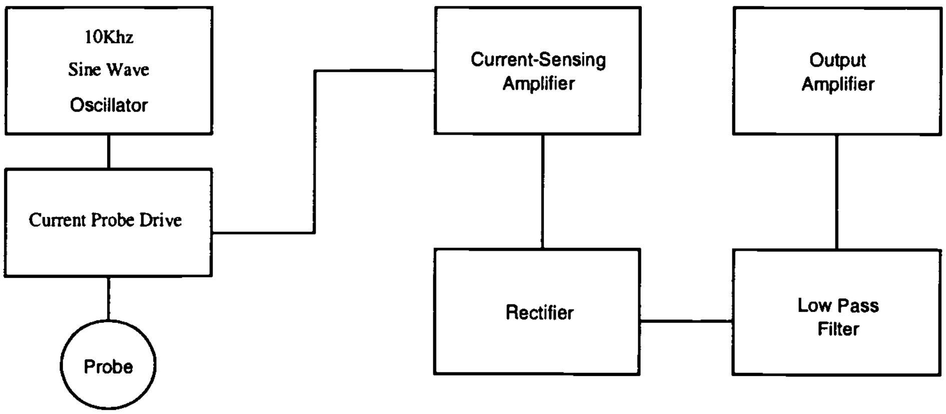

Figure 17. Ring probe circuit design.

5.4. Data Acquisition/Processing

While it is desirable to collect and process data using only one system, time did not allow for the development of a LabVIEW program [16] to acquire data from all of the instruments in the separate effects facility. Therefore, the data acquisition system already in place was used instead of LabVIEW. A FLUKE Hydra Data Bucket, along with the FLUKE software, was used to collect and save the raw voltage signals and their time stamp to the computer. This system can only sample at a maximum frequency of 2Hz for one channel, but is extremely easy to set up and use (described previously in chapter 4 for data acquisition from the capacitance probe). Also, since the other instruments in use in the separate effects facility are configured for the FLUKE Hydra Data Bucket, data acquisition is simplified. For certain transient conditions in the test, aliasing of the sampled data may occur since the maximum scan rate is only twice per second. The desired scan frequency for a particular test should be determined and the appropriate data acquisition system used.

5.5. Cross-Calibration With the Single-Sensor Probe

Because of the gamma-densitometer unavailability, the half-ring probe was instead cross-calibrated with the single-sensor conductivity probe in a vertical air-water system. A picture of this experimental setup is shown in Figure 18.

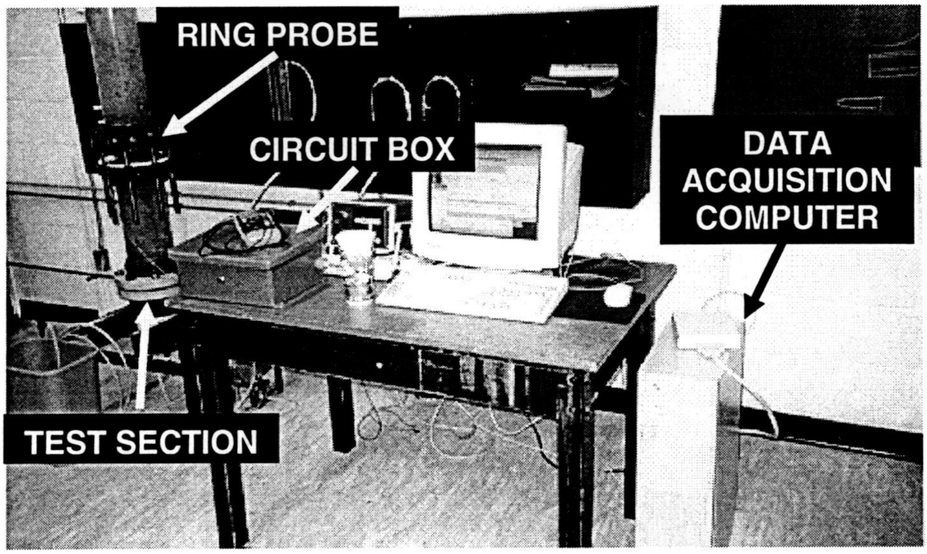

Figure 18. Experimental configuration.

5.5.1. Test Section

The test facility, as described previously in Chapter 3 and pictured in Figures 8 and 18, was designed to simulate level swell phenomena as observed within Oregon State University's (OSU) Advanced Plant Experiment (APEX).

The experiment consisted of a vertical, cylindrical, transparent test section having an inner diameter of 6 in. (15.2 cm). It includes a lower plenum mixing chamber with separate air and water inlets. The parameters measured included air flow rate, collapsed liquid level, and local void fraction from the single-sensor conductivity probe. The collapsed liquid level was measured using a differential pressure cell. The fluid mixture level was measured using a fixed scale for visual indication. A traversing, single-sensor, conductivity probe was used to obtain an area-averaged measurement of the local void fraction over a range of inlet air flow rates and initial collapsed water levels. The results from the area-averaged single-sensor probe data was then used to correlate the output voltage data from the ring probe so that it can be used to determine area-averaged void fraction (for this particular experiment – not applicable to direct application in the LESET experiment).

Area-averaged void fraction for collapsed water levels of 19 in. and 34 in. is presented in Figure 19 as obtained previously with the single-sensor probe.

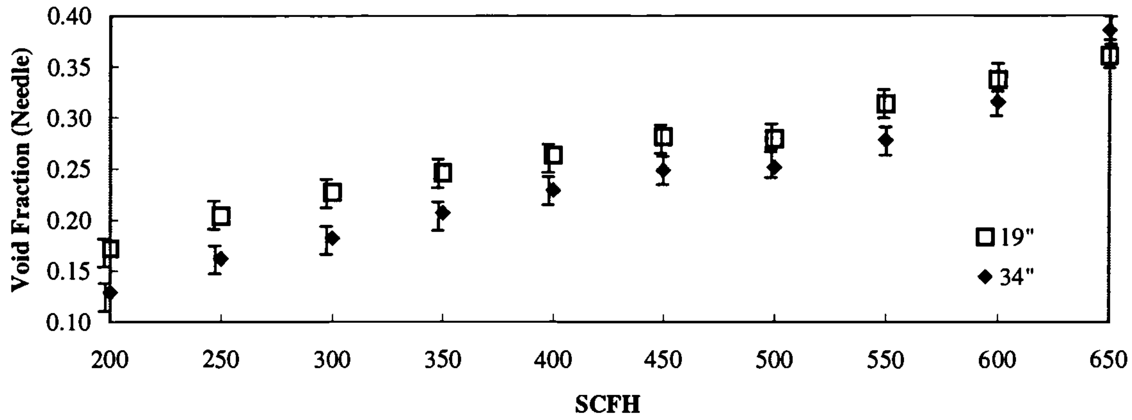

Figure 19. Void fraction for two collapsed water levels versus air flow rate.

As shown above, there is a "plateau," or a region where the void fraction doesn't increase with air flow rate, from 400 to 550 Standard Cubic Feet per Hour (SCFH). This may be due to a flow regime transition from bubbly-to-slug since this change does occur around a void fraction of 25 %. The single-sensor probe data above has a difference of approximately 10% as compared to visual data.

5.5.2. Half-Ring Probe Data

The data from the ring probe was also collected for the same conditions as above. Data was collected at 2 Hz. for 1 minute at each air inlet flow rate. The probe output voltage is plotted as a function of air inlet flow rate. This is shown in Figure 20.

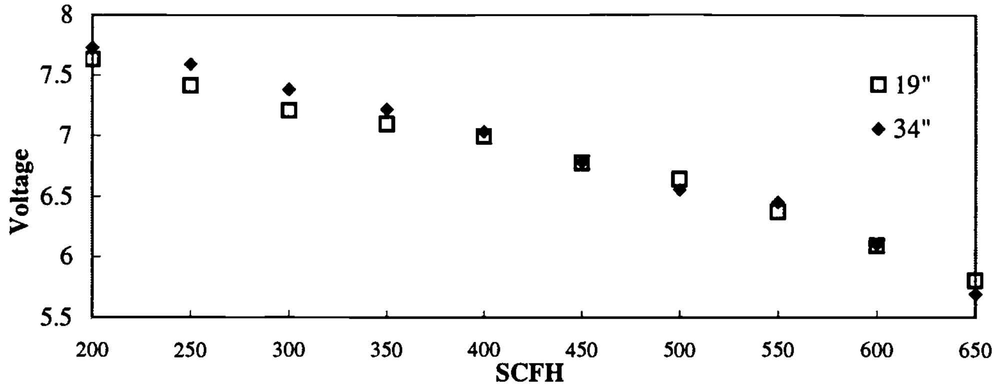

Figure 20. Ring probe voltage output vs. inlet air flow rate.

If Figure 20 is inverted so that the inverse of the voltage is plotted versus the air inlet flow rate, a similar profile is observed as that obtained with the single-sensor conductivity probe. This is shown in Figure 21.

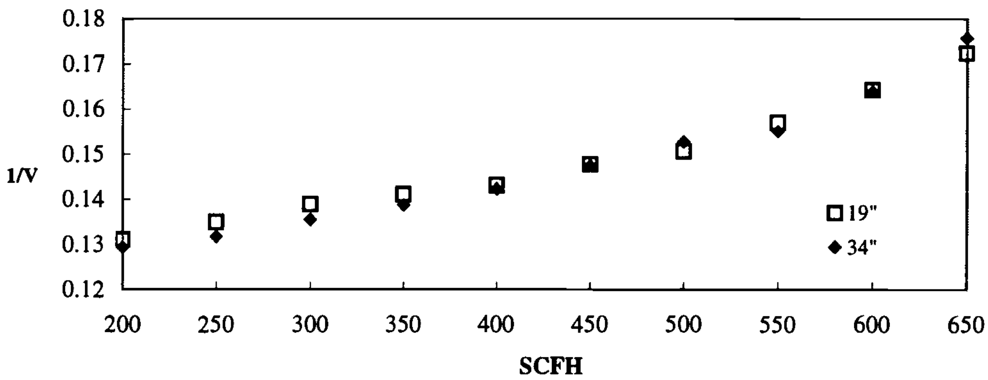

Figure 21. Inverse voltage versus air flow rate.

Figure 19 is very similar to Figure 21. It also shows the "plateau" trend, indicating that the output voltage from the half-ring probe may be directly related to the void fraction in the experiment. Figure 22 shows a radial profile of void fraction as obtained with the single-sensor conductivity probe for varying air inlet rates. The bold colors in the following plot are the flow rates where the flow transition occurs.

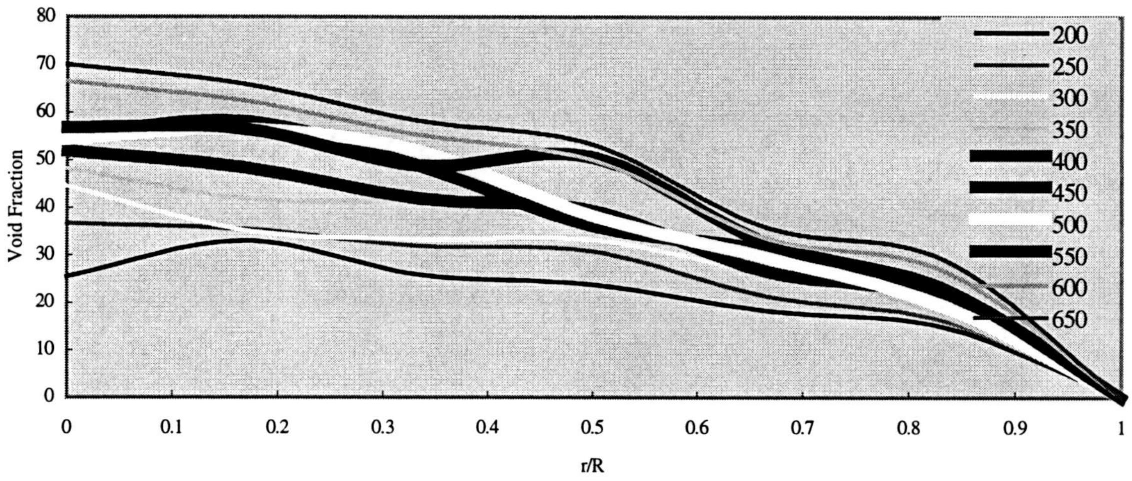

Figure 22. Radial profile of void fraction (from single-sensor probe).

5.5.3. Results

If the data from the two instruments are plotted together such that the area-averaged void fraction (as measured with the single-sensor probe) is plotted versus the voltage output from the ring probe (for the same air flow rate), the final results generated can be shown in Figure 23.

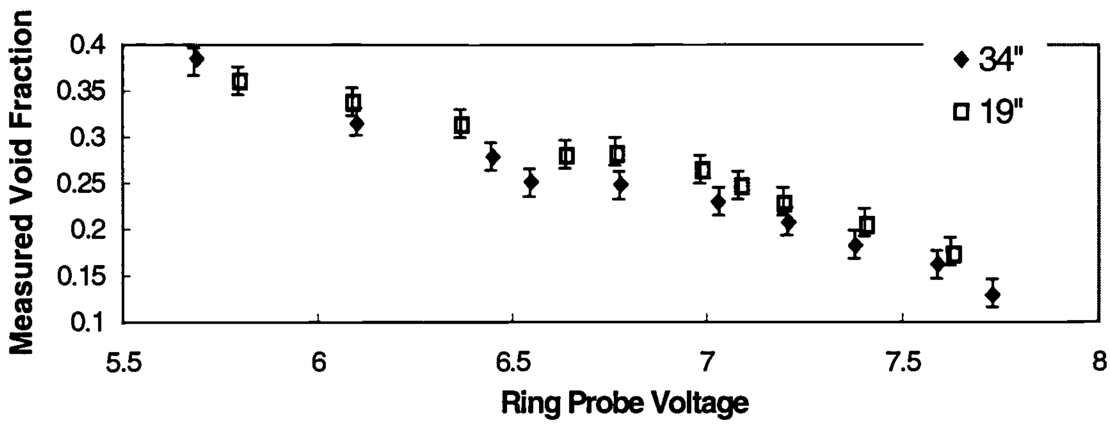

Figure 23. Final cross-calibration.

6. DRAWBACKS AND RECOMMENDATIONS FOR FUTURE RESEARCH

The major shortcomings of the two sensor designs described in this paper are explained and suggestions are offered for future research. Common problems related to intrusive probes in general will be discussed, then drawbacks inherent with each of the two instruments will be presented. Future research is then proposed.

6.1. Drawbacks Inherent With Both Probes

The best instrument in obtaining two-phase flow data is one that minimally disrupts the flow field. LDA, MRI, gamma densitometer systems, and bubble acoustic spectroscopy are totally non-intrusive. As stated previously, these may be impractical owing to budgetary issues, test medium, etc. The single and double-sensor needle probes may significantly disrupt the medium depending on the relative size of the probe to the test section and particle distributions (bubbles). The half-ring probe minimally disrupts the flow field, owing to the flanges necessary for insertion of the probe, and also for the exposed wires inlaid in the PVC. Also, since both of these probes use steel as electrodes, corrosion will occur. The single-sensor probe described in this thesis has successfully been used with the DC power supply for over 50 hours with little signal degradation. Finally, since the probe measurements are time and area-averaged, a sufficient number of samples must be taken to reduce the deviation and standard error.

6.2. Drawbacks Inherent With the Needle-Type Probes

There are some specific issues that need to be addressed with the needle-type probes. From voltage vs. time plots, it is not clearly identified when the bubble enters and leaves the probe tip as shown in Figure 24. The leading edge of this plot is sloped, and the trailing edge of the signal is sloped as well. This is due to the bubble being deformed as the needle penetrates it. It is therefore important to make the probe as non-intrusive as possible, and minimize the exposed tip length. The voltage threshold levels for determining the proper phase may be found in [30]. The measurement of void fraction or bubble velocity may not be very accurate if the bubble size is small enough so that the surface tension is high. The probe employed here has successfully measured void fraction from bubbles with a diameter greater than 3mm (determined visually). Also, if the two-sensor probe is being used for bubble velocity measurements, it is necessary that the probe tips are aligned parallel with the mean flow direction. Obtaining local data and then area-averaging this data may prove to be very time-consuming if sampling time is large and the desired probe mesh spacing is small.

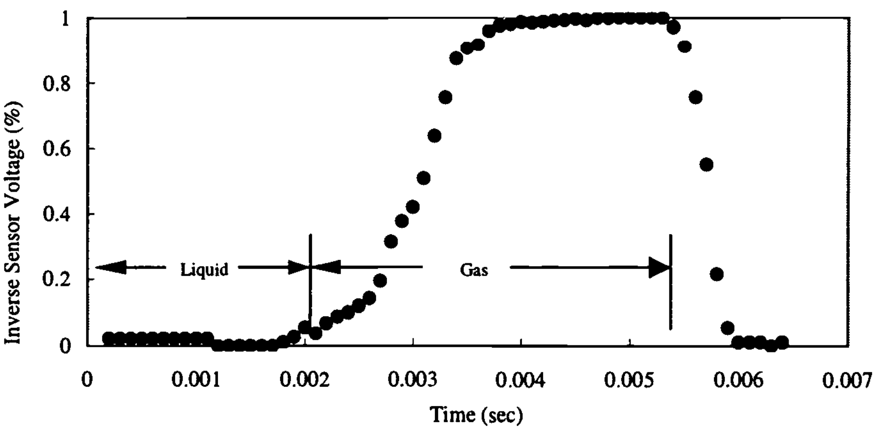

Figure 24. Plot of sensor voltage vs. time.

6.3. Drawbacks Inherent With the Half-Ring Probe

The half-ring probe is relatively new and there are many aspects that need to be further studied. This probe relies on the absolute conductivity of the system, whereas the needle-type probes rely on the relative difference in conductivity of the two phases. Therefore, certain factors need to be quantified that could potentially affect a conductivity change over that data sampling time. If this conductivity does change, a method must be established to correct for this. One factor that plays a significant role in the measured conductivity is the effect of temperature. In the LESET facility for phase separation in tees, the water will heat up over time from the pump as well as frictional effects. Since air is also injected in from an outside tank usually at a different temperature than the water, this may change the conductivity as well. All of these processes must be accounted for during a test. It is proposed that a benchmark curve be performed before a test as well as after a test.

The half-ring probe is not entirely a planar area-average. There is a finite volume over which it measures conductivity. For the system outlined previously, this region was experimentally determined to extend +/- 3 in. beyond the electrodes, and should be studied further. The region size is due mainly to the current generated by the circuit and also the conductivity of the system.

Overall, these drawbacks may be minor depending on the desired measurement parameters. The two instruments described in this thesis are simple and reliable. The total cost for both of these instruments along with a single data acquisition computer and necessary software is only approximately $4,000. This is relatively inexpensive compared to $75,000 LDV systems and $35,000 gamma densitometer systems.

6.4. Recommendations for Future Research

Additional theoretical development and tests are needed to study the interacting electric fields in the half-ring probe, and also the variables affecting conductivity change over sampling time for this probe. A more detailed cross-calibration of the half-ring probe is recommended with the gamma densitometer instead of with the traversing single-sensor probe.

7. CONCLUSIONS

In conclusion, two techniques for measuring two-phase flow parameters in an air/water system using intrusive conductivity probes were presented. The process of constructing single-sensor and double-sensor needle type probes was explained. A typical procedure to collect and process void fraction information from a single-sensor probe was given, and then results of an experimental effort to benchmark this probe against other techniques was presented. The theoretical derivation for measuring void fraction and interfacial area using a two-sensor needle-type probe, as well as a statistical analysis of the accuracy using the two-sensor probe for measuring interfacial area was determined from a comprehensive literature review. A second technique to measure void fraction in air/water flows is with a half-ring type conductivity probe. It was demonstrated that this half-ring probe can measure a global void fraction when cross-calibrated with the area-averaged single-sensor probe void fraction data. The two techniques discussed (needle and ring type probes) are accurate, simple, reliable, and inexpensive compared to other void fraction measurement devices.

8. REFERENCES

1. Wallis, G.B., *One-Dimensional Two-Phase Flow*, McGraw-Hill Book Company, New York, NY. 1969.

2. Ishii, M. and Mishima, K., Study of Two-Fluid Model and Interfacial Area. ANL-80-111, NUREG/CR-1873. Argonne National Laboratory. 1980.

3. Taitel, Y. and Dukler, A.E., A Model for Predicting Flow Regime Transitions in Horizontal and Near Horizontal Gas-liquid Flow. *AIChE Journal*, **22**, 1976. pp. 47.

4. Ishii, M., *Thermo-Fluid Dynamic Theory of Two-Phase Flow*, Collection de la Direction des Etudes et Recherches d'Electricite de France, Eyrolles, Paris, 1975.

5. Kocamustafaogullari, G., and Ishii, M. Interfacial Area and Nucleation Site Density in Boiling Systems. *Int. J. Heat and Mass Transfer,* **26**, No. 9. 1983. p. 312.

6. Ishii, M., Wu, Q., Kim, S., Assad, A., and McCreary, D., Studies on Interfacial Area Transport Phenomena of Two-Phase Flow in Vertical Duct, PU NE 98-4, 1998.

7. Ishii, M. and Kojasoy, G., Interfacial Area Transport Equation and Preliminary Considerations on Closure Relations. PU NE-93/6, Purdue University Report. 1993.

8. Kataoka, I., Ishii, M., and Serizawa, A., Local Formulation and Measurements of Interfacial Area Concentration in Two-phase Flow. *Int. J. Multiphase Flow*, 1986, **12** No. 4, 505-512.

9. Wu, Q., Kim, S., McCreary, D., Ishii, M., and Beus, S.G. (Bettis Atomic Power Lab), Measurements of Interfacial Area Concentration in Two-Phase Bubbly Flow, ANS 1997 Winter Meeting, Nov. 16-20, TANSAO 77, 1997. p. 437.

10. McCreary, D., Laser Doppler Anemometry Theory and Applications, Purdue University, Department of Nuclear Engineering, 1998.

11. Whitelaw, J.H., "Laser Velocimetry: Problems and Opportunities" *Engineering Applications in Laser Velocimetry*, ASME Winter Annual Meeting, Phoenix, Arizona, November 1982.

12. Kim, S., Fu, X. Y., Wang, X., and Ishii, M., Development of the Miniaturized Four-Sensor Conductivity Probe and the Signal Processing Scheme, accepted by Int. J. Heat Mass Transfer, Jan. 2000.

REFERENCES (Continued)

13. Neal, L. G. and Bankoff, S. G., "A High Resolution Resistivity Probe for Determination of Local Void Properties in Gas-Liquid Flow", *A.I.Ch.E.J.*, **9**, pp. 490-494, 1963.

14. Kim, S., Wu, Q., and Ishii, M., Fabrication Procedure and Design of a Double-Sensor Conductivity Probe, PU NE 97-1, 1997.

15. McCreary, D., Characterization and Performance of a Single-Sensor Conductivity Probe for the Measurement of Local Time-Averaged Void Fraction, Oregon State University-ATHRL-98001 Report, February 1999.

16. LabVIEW User Manual, Part Number 320999B-01, January 1998.

17. Ellis, C., McCreary, D., Wu, Q., and Reyes, J., "Assessment of Level Swell Models in an Air-Water System", submitted to NURETH-9 Conference, 1999.

18. Ellis, C., Characterization and Performance Testing on a Drexelbrook 408-8200 (Universal II™) Series Level Transmitter, Oregon State University-ATHRL-99005 Report, February 1999.

19. Kataoka, I. and Ishii, M., Drift Flux Model for Large Diameter Pipe and New Correlation for Pool Void Fraction. *Int. J. Heat and Mass Transfer,* **30**, pp. 1927-1939. 1987.

20. Boesmans, B., and Berghmans, J., Level Swell in Pool Boiling with Liquid Circulation. *Int. Journal of Heat and Mass Transfer* **38**, 989-997. 1994.

21. Wu, Q. and Ishii, M., Sensitivity Studies on Double-sensor Conductivity Probe for the Measurement of Interfacial Area Concentration in Bubbly Flow. *Int. J. Multiphase Flow*, 1998. **25**, 155-173.

22. Revankar, S. and Ishii, M., Local Interfacial Area Measurement in Bubbly Flow. *Int. J. Heat and Mass Transfer*, 1992, **35**, 913-925.

23. Kataoka, I., Ishii, M., and Serizawa, A., Sensitivity Analysis of bubble Size and Probe Geometry on the Measurements of Interfacial Area Concentration in Gas-liquid Two-phase Flow. *J. Nuclear Engr. & Design*, 1994, **146**, 53-70.

24. Leung, W. H., Modeling of Interfacial Area Concentration and Interfacial Momentum Transfer: Theoretical and Experimental Study. Ph. D. Thesis, Dept. of Nuclear Engineering, Purdue University, West Lafayette, U.S.A., 1996.

REFERENCES (Continued)

25. Wu, Q., Welter, K., and McCreary, D., Bubble Velocity Distributions in Two Phase Bubbly Flow, Conference Proceedings, NURETH-9, 1999.

26. Reyes, J.N., "Phase Separation in Tees" proposal submitted to NRC from Department of Nuclear Engineering, Oregon State University. 1997.

27. Schrock, V.E., Revankar, S.T., and Mannheimer, R., Small Break Discharge - The Roles of Vapor and Liquid Entrainment in a Stratified Two-Phase Region Upstream of the Break. NUREG/CR-4761, LBL-22024. 1986.

28. Todreas, N.E. and Kazimi, M.S., *Nuclear Systems I: Thermal Hydraulic Fundamentals*. Taylor & Francis, Bristol, PA 19007, USA. 1989.

29. Dibble, T. and Sollitt, C., "New Designs for Acoustic and Resistive Wave Profilers", O.H. Hinsdale Wave Research Laboratory, Oregon State University.

30. Dias, S., Franca, F., and Rosa, E., A generalized Approach to Estimate the Size and Velocity Distributions of Spherical Bubbles Using Intrusive Crossing ProbesExperimental Heat Transfer, Fluid Mechanics and Thermodynamics, 1997, 957-970.